Bibliographical reference

Time-Domain Modelling: Combining ESM and FDTD Methods for Acoustic Wave Propagation, Stig Kleiven, Krister Larsson and Wolfgang Kropp, Acta Acustica **vol. 95** (Number 1), 2009, pp. 118-127

DOI
https://doi.org/10.3813/AAA.918133

Acta Acustica united with Acustica
Vol. 95 (2009) 118 – 127

DOI 10.3813/AAA.918133

Time-Domain Modelling: Combining ESM and FDTD Methods for Acoustic Wave Propagation

Stig Kleiven, Krister Larsson, Wolfgang Kropp
Division of Applied Acoustics, Chalmers University of Technology, SE-412 96 Göteborg, Sweden.
Stig.kleiven@chalmers.se

Summary
Time-domain modelling of acoustic wave propagation is computationally expensive, escpecially in applications with large differences in length scales, such as thermoacoustic devices. Thus, there is a need for efficient modelling solutions. One possibility is to combine the established time-domain methods with more efficient methods. The aim of this paper has been to develop a time-domain model combining the equivalent source method (ESM) and the finite-difference time-domain (FDTD) method. The idea was to model the complex acoustic fields using FDTD method and the less complex fields using ESM. These methods were coupled by ensuring continuity of volume velocity and pressure at the boundary between them. Simulations with the combination of the methods were compared to analytical and experimental results, and shown to be accurate and numerically stable for 1-D energy flow, including viscous attenuation. Furthermore, the combination proved significantly quicker than using only the FDTD method. Combining ESM and FDTD has potential as a computationally efficient alternative compared to the latter alone.

PACS no. 43.20.El, 43.20.Mv

1. Introduction

Time-domain modelling, in contrast to frequency-domain modelling, has the advantage to study time-varying boundary conditions and non-linear effects. Therefore, time-domain modelling of thermoacoustic devices [1, 2], which are mainly simulated using frequency-domain methods [3], can be beneficial. Thermoacoustic devices, heat pumps or engines, basically consist of a stack of plates placed in a resonator. The length of the resonator is of the order of the acoustic wavelength λ of the fundamental frequency, whereas the stack spacing is of the order of the thermal penetration depth δ. The relation λ/δ is typically of the order of 10^4 (for 200 Hz at 1 atm air at 20°C). This large difference in length scales is a challenge in time-domain modelling, since it requires a small spatial and time resolution leading to a large computational mesh and a high computational cost. One way to reduce the computational cost is to combine two methods; a detailed method for the small geometries in the stack and a quicker method for the duct parts outside the stack. An appropriate detailed method for the small geometries in the stack is the finite-difference time-domain (FDTD) method.

In recent years, there has been an increasing interest in FDTD modelling in acoustics, e.g. [4, 5]. The FDTD method is simple to implement as well as enabling the study of transients, non-linear effects and time-varying boundary conditions. Disadvantages of the FDTD method are the inability to model curved geometrical boundaries and the high computational costs. In order to overcome these disadvantages FDTD has been combined with other methods.

In electromagnetics, FDTD has been combined with the finite-element method in time domain (FETD) in order to improve modelling of curved boundaries [6, 7]. In acoustics, the combination of FETD and FDTD has recently been used to model frequency dependant reflections and absorption of surfaces [8]. However, FETD is computationally more expensive than FDTD. In the outdoor sound propagation field, Renterghem *et al.* combined FDTD with the quicker parabolic equation (PE) model [9]. They modelled the region close to the source, where a high level of detail was required, using FDTD, while the region far away from the source was modelled using PE. Since PE is a frequency-domain method, a complete time-domain simulation is not possible with the combination of the FDTD method and the PE model.

A simple and computational efficient method appropriate for for the duct parts outside the stack, is the equivalent source method (ESM). The ESM, also known as source simulation or substitute sources, has been used widely in the modelling of acoustic problems, e.g. [10, 11]. A detailed study of the properties and limitations of ESM can be found in [12]. Contrary to the usual frequency-domain formulations, Kropp *et al.* developed a time-domain formulation of the ESM [13, 14].

Received 23 May 2008, revised 25 October 2008,
accepted 28 October 2008.

The purpose of this paper was to combine FDTD with the faster time-domain ESM in order to reduce the total computational cost. The study was restricted to 1-D wave propagation, although 2-D effects such as shear forces in the transverse direction were included. No heat or thermal effects were included, hence this study was focused on the coupling between the two methods. First the two methods, ESM and FDTD, are described separately. Thereafter, the coupling procedure is presented for 1-D and 2-D FDTD grids. Numerical errors and computational efficiency are discussed before a simulation example of a duct containing a segment with viscous attenuation is compared with experimental and analytical results.

2. FDTD for 1-D acoustic plane waves

The FDTD method is well-established, e.g. [15, 16], thus the method applied to acoustic plane wave propagation is only briefly presented here. The 1-D acoustic adiabatic plane wave propagation in a lossless medium in a duct with uniform cross-section S is described by the momentum equation and the equation of continuity,

$$\frac{\partial p}{\partial t} = -c^2 \frac{\rho}{S} \frac{\partial U}{\partial x}, \tag{1}$$

$$\frac{\partial U}{\partial t} = -\frac{1}{\rho/S} \frac{\partial p}{\partial x}, \tag{2}$$

where p is the acoustic pressure, U is the volume velocity, ρ is the density in the medium, c is the speed of sound, t is the time and x is the space variable. These equations can be discretised using the second-order Yee FDTD method [17]. Using this method, the pressure and volume velocity are discretised with alternating position and time. The pressure calculated with central finite-difference at time step $n\Delta t$ and position $i\Delta x$ (denoted n and i for simplicity) is

$$p_i(n+1/2) = p_i(n-1/2) - c^2 \frac{\rho}{S} \frac{\Delta t}{\Delta x} \left[U_{i+\frac{1}{2}}(n) - U_{i-\frac{1}{2}}(n) \right], \tag{3}$$

and the volume velocity calculated with finite difference at time step $(n+1/2)\Delta t$ and at position $(i+1/2)\Delta x$ is

$$U_{i+\frac{1}{2}}(n+1) = U_{i+\frac{1}{2}}(n) - \frac{1}{\rho/S} \frac{\Delta t}{\Delta x} \left[p_{i+1}(n+1/2) - p_i(n+1/2) \right], \tag{4}$$

where Δt and Δx are the time step and space increment in the discretisation.

The choice of the space increment Δx and the time step Δt is essential, regarding numerical stability and dispersion. FDTD is stable if the Courant number $S_c = \frac{c\Delta t}{\Delta x} \leq 1/\sqrt{\dim}$ [15], where "dim" is the number of spatial dimensions. Using $S_c = 1$ in the discretisation of 1-D wave equations, no matter how coarse the discretisation is, Taflove *et al.* have shown that FDTD gives the exact solution [15]. However, for a Courant number lower than one, numerical dispersion occur. The influence of the dispersion in the coupling between ESM and FDTD methods will be further discussed in section 4.

In FDTD the chosen source function is usually smooth, e.g. a Gaussian pulse, in order to avoid spurious noise in higher frequencies. However, in this paper we use a unit pulse as a source in the ESM part, since all frequencies up to the Nyquist rate ($\frac{1}{2\Delta t}$) are included with equal strength. Thus, the coupling can be studied in the whole frequency range. Source implementation in the FDTD part and corresponding source scattering are out of the scope of this paper, since we focus on the coupling between FDTD and ESM.

3. Equivalent Source Method (ESM)

In this section, we present the time-domain ESM for plane waves in a duct. First the formulation for one duct segment is shown, and thereafter the system of equations for combinations of different duct segments is presented.

In ESM, the object of interest is divided into subparts with simple geometry, in which each subpart can be described by a Green's function. Equivalent sources are placed at the boundaries, so that the problem is reduced to finding the strength of these sources in order to fulfil the boundary conditions. The various steps in the method are described in the following.

3.1. Single segment

A segment in ESM is usually described as a rigid cavity using a Green's function including all the reflections. In this paper, we describe the acoustic field in a duct segment by two opposite travelling plane waves. For a segment with length L and cross section S, the acoustic field in the frequency domain is (omitting $e^{j\omega t}$)

$$p(x,\omega) = \frac{\rho c}{S} q_1(\omega) e^{-jkx} + \frac{\rho c}{S} q_2(\omega) e^{-jk(L-x)} \tag{5}$$

$$U(x,\omega) = q_1(\omega) e^{-jkx} - q_2(\omega) e^{-jk(L-x)}, \tag{6}$$

where p is the pressure, U is the volume velocity, ρ is the density, c is the sound speed, q_1 and q_2 are the amplitudes of the volume velocities of the two waves, and k is the wave number. Damping may be included by having a complex k. In the time domain, equations (5) and (6) correspond to

$$p(x,t) = \frac{\rho c}{S} q_1(t) * g_1(t,x) + \frac{\rho c}{S} q_2(t) * g_2(t,x) \tag{7}$$

$$U(x,t) = q_1(t) * g_1(t,x) - q_2(t) * g_2(t,x), \tag{8}$$

where $g_1(t)$ and $g_2(t)$ are the inverse Fourier transforms of e^{-jkx} and $e^{-jk(L-x)}$, respectively, which correspond to delayed Dirac functions. The convolutions, denoted with "$*$", can be written in discrete time as

$$\begin{aligned} q_i(n\Delta t) * g_i(n\Delta t, x) &= \sum_{k=0}^{n} q_i(k\Delta t) g_i((n-k)\Delta t, x) \\ &= q_i(n\Delta t) g_i(0,x) + \sum_{k=0}^{n-1} q_i(k\Delta t) g_i((n-k)\Delta t, x), \end{aligned} \tag{9}$$

where $n\Delta t$ is the current time step. The first term on the right-hand side corresponds to the current value and the second term consists only of known values from the past.

Assuming that the dimensions of the duct and the media properties are known, the only unknowns are the source strengths q_1 and q_2. These source strengths can be determined from the boundary conditions.

3.2. Combining segments

Two segments, as shown in Figure 1, are combined by using the formulation for a single segment, section 3.1, and by ensuring that the boundary conditions and continuity of pressure and volume velocity are fulfilled.

Four equations, expressing the boundary conditions, are necessary to calculate the four unknown equivalent sources. The equations for the duct in Figure 1 for a given volume source and a hard end are given by the following equations in the frequency domain:

$$q_{a,1} - q_{a,2}\mathrm{e}^{-\mathrm{j}k_aL_a} = q_s, \tag{10}$$

$$q_{a,1}\mathrm{e}^{-\mathrm{j}k_aL_a} - q_{a,2} = q_{b,1} - q_{b,2}\mathrm{e}^{-\mathrm{j}k_bL_b}, \tag{11}$$

$$\frac{\rho_a c_a}{S_a}\Big(q_{a,1}\mathrm{e}^{-\mathrm{j}k_aL_a} - q_{a,2}\Big) = \frac{\rho_b c_b}{S_b}\Big(q_{b,1} - q_{b,2}\mathrm{e}^{-\mathrm{j}k_bL_b}\Big), \tag{12}$$

$$q_{b,1}\mathrm{e}^{-\mathrm{j}k_bL_b} - q_{b,2} = 0, \tag{13}$$

where q_s is the given volume source. Equation (10) states that the volume velocity equals the external source at the left end, (11) and (12) state the continuity of volume velocity and pressure at the boundary between the segments, and (13) states that the volume velocity equals zero at the hard end.

Equations (10)–(13) are transformed to the time domain, as described in section 3.1, and rearranged to place the four unknown equivalent sources at the current time step at one side. Furthermore, the inverse Fourier transform of $\mathrm{e}^{-\mathrm{j}kL_a}$ is denoted g_a and we use the inverse Fourier transform of $\mathrm{e}^{-\mathrm{j}k\cdot 0}$ corresponding to a non-delayed unit pulse, which equals one at the current time step. We then have a system of equations in matrix form that has to be solved at every time step:

$$\big[\mathbf{M}\big]\mathbf{V} = \mathbf{R}, \tag{14}$$

where

$$[\mathbf{M}] = \begin{bmatrix} 1 & -g_a(0) & 0 & 0 \\ g_a(0) & -1 & -1 & g_b(0) \\ \frac{\rho_a c_a}{S_a} g_a(0) & \frac{\rho_a c_a}{S_a} & -\frac{\rho_b c_b}{S_b} & -\frac{\rho_b c_b}{S_b} g_b(0) \\ 0 & 0 & g_b(0) & -1 \end{bmatrix},$$

$$\mathbf{V} = \begin{bmatrix} q_{a,1}(n\Delta t) \\ q_{a,2}(n\Delta t) \\ q_{b,1}(n\Delta t) \\ q_{b,2}(n\Delta t) \end{bmatrix},$$

$$\mathbf{R} = \begin{bmatrix} q_s(n\Delta t) + A_{a,2} \\ -A_{a,1} - A_{b,2} \\ -\frac{\rho_a c_a}{S_a} A_{a,1} + \frac{\rho_b c_b}{S_b} A_{b,2} \\ -A_{b,1} \end{bmatrix},$$

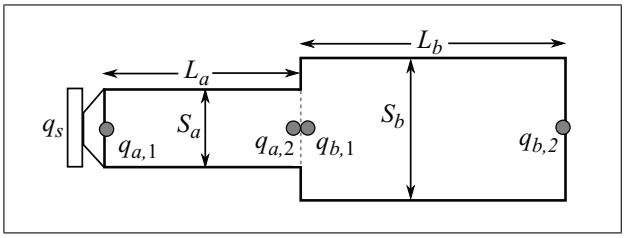

Figure 1. A duct consisting of two parts with different length and cross-section. Source at the left end.

where $A_{i,j}$ contains the values from the previous time steps

$$A_{i,j} = \sum_{k=0}^{n-1} q_{i,j}(k\Delta t) g_i\big((n-k)\Delta t\big). \tag{15}$$

Similarly, an arbitrary number of segments can be combined using ESM. The next section describes how to combine ESM and FDTD.

4. Coupling between ESM and FDTD

In the coupling between ESM and FDTD the idea is to ensure the continuity of volume velocity and pressure at the boundaries, similar to the combination of segments using ESM, described in section 3.2. In addition, the alternating time steps between pressure and volume velocity in the FDTD method have to be taken into account. First, the coupling between 1-D ESM and 1-D FDTD is described; secondly, the coupling is expanded to include 2-D FDTD. Finally, numerical errors and computational efficiency are discussed.

4.1. Coupling between 1-D ESM and 1-D FDTD

The equivalent sources and the pressure and volume velocity grid points (see in Figure 2) are coupled by continuity of volume velocity and pressure at the boundary. The cross-sections are denoted S_a in the ESM part and at $i = 1$ in the FDTD part, whereas the cross-section in the FDTD part for $i \geq 2$ is denoted S_b. The cross-section at $i = 3/2$ is still undefined, hence also the impedance, $Z_{i=3/2} = \rho c/S_{i=3/2}$. The impedance $Z_{i=3/2}$ can be defined by the average of the impedances at $i = 1$ and $i = 2$, which gives the following expression for the cross-section $S_{i=3/2}$

$$\begin{aligned} Z_{i=3/2} &= \frac{1}{2}\big(Z_{i=1} + Z_{i=2}\big) \\ \frac{\rho c}{S_{i=3/2}} &= \frac{1}{2}\Big(\frac{\rho c}{S_a} + \frac{\rho c}{S_b}\Big) \\ \Rightarrow S_{i=3/2} &= 2\Big(\frac{1}{S_a} + \frac{1}{S_b}\Big)^{-1}, \end{aligned} \tag{16}$$

since the density ρ and speed of sound c are assumed to be constant.

The alternating position and time in the FDTD method are taken into account by calculating the pressure at the boundary using the equivalent volume source located half a spatial step away from the previous half time step. The procedure of the coupling is described in the following.

The procedure of 1-D coupling

The coupling consists of four calculation steps in each time step. These four steps are described below.

1. The pressure $p_i(n - 1/2)$ is calculated for all FDTD grid positions using equation (3) with $S = S_b$, except for the position $i = 1$ at the interface between the FDTD and ESM parts.
2. In order to ensure continuity of pressure at the boundary, $p_1(n-1/2)$ is set equal to the pressure from the ESM parts,

$$p_1(n - 1/2) = \frac{\rho c}{S_a}\big(A_1 + q_2(n - 1)\big), \tag{17}$$

where A_1 contains known values from the past convolution,

$$A_1 = \sum_{k=0}^{n-1} q_1(k)g(n - k). \tag{18}$$

3. $U_{i+\frac{1}{2}}(n)$ is calculated for all the FDTD grid positions, using equation (5) with $S = S_b$, except for the position $i = 3/2$ where $1/S = (1/S_a + 1/S_b)/2$ as shown in equation (16). $U_{\frac{3}{2}}(n)$ is used in the next step of the procedure (step 4).
4. The equivalent volume sources are calculated from the continuity of volume-flow at the boundaries, by solving the system of equations

$$\mathbf{V} = [\mathbf{M}]^{-1}\mathbf{R}, \tag{19}$$

where

$$[\mathbf{M}] = \begin{bmatrix} 1 & -g(0) \\ g(0) & -1 \end{bmatrix}, \quad \mathbf{V} = \begin{bmatrix} q_1(n) \\ q_2(n) \end{bmatrix},$$
$$\mathbf{R} = \begin{bmatrix} q_s(n) + A_2 \\ U_{\frac{3}{2}}(n) - A_1 \end{bmatrix},$$

q_s is the source located at the same position as the equivalent source q_1 and A_2 is

$$A_2 = \sum_{k=0}^{n-1} q_2(k)g(n - k). \tag{20}$$

Then the same procedure is carried out for the following time steps.

4.2. Coupling between 1-D ESM and 2-D FDTD

The coupling is expanded to include a 2-D grid in the FDTD part, keeping the ESM part one-dimensional. In the FDTD part, as in the ESM part, wave propagation is restricted to the x-direction along the duct. Thus, only the x-component of the velocity is included, assuming the y-component of the velocity to be negligible. The x-component of the velocity is allowed to vary with both position (x, y) and time t. The velocity at the transverse boundaries is decided from the boundary conditions.

Since these assumptions also imply only volume flow in the x-direction, we calculate sub-volume velocities, $\hat{U} = \Delta S \cdot u$, in the FDTD part. $\Delta S = S/(N_y - 2)$ and N_y is the number of grid points in the transverse direction. The expansion to 2-D FDTD, illustrated in Figure 3, gives the following coupling procedure.

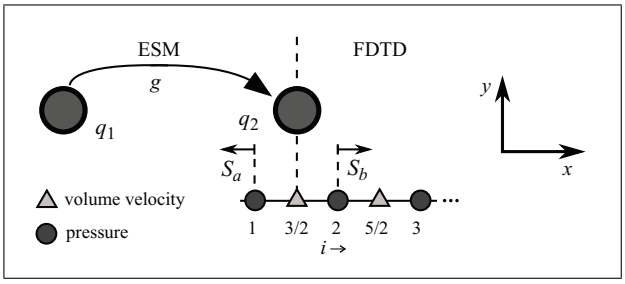

Figure 2. Schematic overview of the coupling between 1-D ESM and 1-D FDTD.

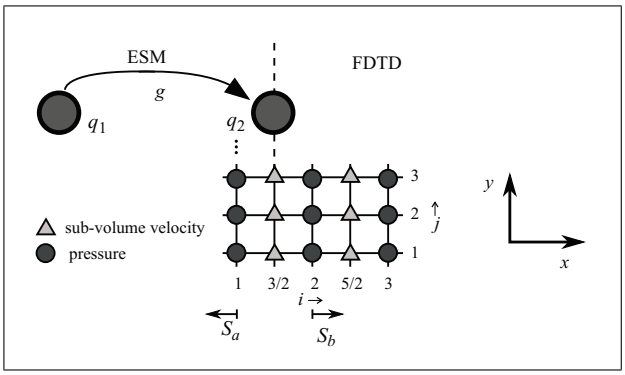

Figure 3. Schematic overview of coupling between 1-D ESM and 2-D FDTD.

The procedure of 2-D coupling

The coupling consists of five calculation steps in each time step. These five steps are described below.

1. The pressure $p_{i,j}(n - 1/2)$ is calculated for all FDTD grid positions with $\Delta S = \Delta S_b = S_b/(N_y - 2)$, except for the position $(i = 1, j)$ at the interface between the FDTD and ESM parts.
2. In order to ensure continuity of pressure at the boundary, $p_{1,j}(n - 1/2)$ is set equal to the pressure from the ESM parts,

$$p_{1,j}(n - 1/2) = \frac{\rho c}{S_a}\big(A_1 + q_2(n - 1)\big), \tag{21}$$

where A_1 contains known values from the past convolution, equation (18)
3. $\hat{U}_{i+\frac{1}{2},j}(n)$ is calculated for all the FDTD grid positions with $\Delta S = \Delta S_b$, except for the position $(i = 3/2, j)$ where $1/\Delta S = (1/\Delta S_a + 1/\Delta S_b)/2$ and $\Delta S_a = S_a/(N_y - 2)$.
4. The total volume flow $U_{\frac{3}{2}}(n)$ at the boundary $(i = 3/2, j)$ is calculated by summation over the FDTD sub-volume velocity points

$$U_{\frac{3}{2}}(n) = \sum_{\mathrm{j}=1}^{N_y} \hat{U}_{\frac{3}{2},j}(n), \tag{22}$$

$U_{\frac{3}{2}}(n)$ is used in the next step of the procedure (step 5).
5. The equivalent volume sources are calculated. Identical to step 4 in the 1-D coupling procedure.

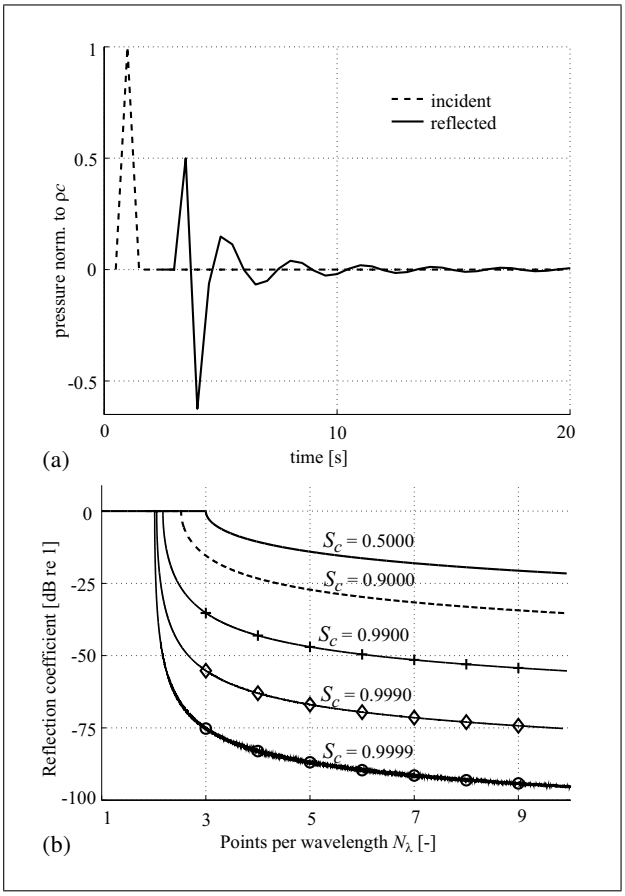

Figure 4. Numerical reflections occurred from the coupling between ESM and FDTD. In (a) the incident and the reflected pulse from the coupling using $S_c = 0.5$, $\Delta x = 1$ m, $c = 1$ m/s, are shown. In (b) the reflection coefficients, calculated from incident and reflected pulses, for different Courant numbers are shown. The reflection coefficients are plotted as a function of points per wave length $N_\lambda = \lambda/\Delta x$.

Since wave propagation is assumed only in one direction for this case, a Courant number $S_c = 1$ can be used. However, if $S_c < 1$ numerical dispersion is introduced in the FDTD part. In the following, it is shown that the dispersion leads to reflections at the boundary between ESM and FDTD.

4.3. Evaluation and numerical reflections

In order to investigate possible numerical errors introduced by the coupling, a duct with constant uniform properties is modelled with the combination of ESM and 1-D FDTD, as in Figure 5. A velocity unit-pulse source is located at the ESM part, and numerical reflections from the coupling are studied. The simulations are stopped before any reflections from the ends of the duct have arrived at the receiver, which is located at Δx from the boundary in the ESM part.

Despite the fact that the impedances in both segments are the same, reflections from the coupling occur for Courant numbers lower than one. The reflected pulse from the coupling with a Courant number $S_c = 0.5$ is seen in Figure 4a. These reflections introduce numerical errors.

For different Courant numbers, the reflection coefficient at the coupling is calculated by dividing the Fourier transform of the reflected pressure signal by the Fourier transform of the incident pressure pulse. In Figure 4b, the reflection coefficients are plotted as a function of points per wave length, $N_\lambda = \lambda/\Delta x$. The plots show that the reflection coefficient, like the numerical dispersion in the FDTD method, increases with lower Courant numbers. Furthermore, the reflections from the coupling decrease with improved resolution (or lower frequency) and there is total reflection below a certain resolution limit, e.g. below 3 points per wave length for $S_c = 0.5$. These total reflection limits coincide with the resolution at which the numerical wave numbers in the FDTD method become complex, as shown by Schneider *et al.* [18].

The complex wave number, together with the alternating time step and position for velocity and pressure, leads to an impedance that varies with frequency in the FDTD part. Since the impedance is constant in the ESM part, this frequency-dependent impedance causes an impedance mismatch leading to numerical reflections. It should be noted that using a Courant number $S_c = 1$, the numerical wave number is constant in the FDTD part and there is no dispersion. No numerical reflections are observed for $S_c = 1$, thus the coupling works.

4.4. Computational efficiency

The computational efficiency of the combination of FDTD and ESM in comparison to using only FDTD is investigated here. In order to study a general behaviour of the computational efficiency, it was investigated as a function of grid size. The computational time for a single time step is calculated for the ESM part and FDTD part.

The ESM part includes a 2x2 matrix inversion, equation (19), and two vector additions in order to store previous values, equations (18) and (20). The matrix inversion can be discarded if the damping is excluded in the ESM part. The computational time for vector additions in the ESM parts increases for a longer duct, since the Green's function becomes longer. The FDTD part includes four N_xx1 vector subtractions, equations (3) and (5), in which the computational time increases with a longer duct, since the number of grid points increase. Approximately, the computational time for FDTD is twice as long for 1-D and N_y as long for 2-D compared to the ESM part

$$CT_{\text{1-D}} = \frac{\text{1-D FDTD}}{\text{1-D ESM}} \approx \frac{4N_x}{2N_x} = 2 \tag{23}$$

$$CT_{\text{2-D}} = \frac{\text{2-D FDTD}}{\text{1-D ESM}} \approx \frac{4N_xN_y}{2N_x} = 2N_y, \tag{24}$$

where CT is computational time.

The simulations are performed in Matlab version 7.2 on a Macintosh G5, 2 GHz CPU and 3 GB memory. The space increment is set to $\Delta x = 1$; the Courant number $S_c = 1$ and the time step Δt are kept constant in all the simulations. The length of the duct is varied, in terms of grid points in FDTD and corresponding length in ESM;

see Figure 5. For 2-D FDTD, a quadratic uniform grid is assumed, hence $\Delta y = \Delta x$ and $N_y = N_x$.

As seen in the Figure 6, the calculation time for the 1-D FDTD part versus the ESM part is approximately twice as long. The computational time for 2-D FDTD is 3-10 times longer for small grids. For grid sizes above 100x100, the computational time is more than 100 times longer and increases by a factor of 2.6 per doubling of N_x. Based on our investigations using different hardware, we believe that the jump at $N_x = 45$ for the computational time for 2-D FDTD relates to how Matlab handles addition and subtraction of matrixes.

5. Example of a duct containing a viscous part

A duct containing a stack, a part consisting of numerous narrow channels, was studied. Since the stack introduces a change in area and viscous attenuation, which cause an impedance shift, reflections from the stack were expected. The reflections were investigated experimentally, analytically and numerically by using the combination of the ESM and 2-D FDTD methods.

5.1. Description of measurements

The experimental setup consisted of a loudspeaker connected to a circular duct, 3618 mm long with an open end. A ceramic stack containing 62 quadratic channels per cm^2 was placed 2660 mm away from the loudspeaker in the duct. The width of the channels, 1.09 mm, and the thickness of the layer between the channels, 0.18 mm, corresponded to an area change of

$$B = \frac{1.09^2}{(1.09 + 0.18)^2} = 0.74. \quad (25)$$

Recordings were made with a microphone located 220 mm away from the loudspeaker, while producing broad-band noise. These measurements were performed for two settings, with and without the stack. Hence, by comparing the impulse responses between the microphone signal and the input signal for the two settings, the reflections from the stack were estimated. A sampling frequency of 51.2 kHz and a frequency resolution of 1.6 Hz were used.

5.2. Measurement results

The first part of the impulse response, with and without the stack, is seen in Figure 8a. The incident pulse from the loudspeaker reached the microphone at approximately 1 ms. The peak at 15 ms was the first reflection from the stack. Furthermore, the open-end reflections for the two cases arrived at different time steps, 20 ms and 21 ms, since the total length of the duct was shorter when the stack was removed.

Subtracting the two impulse responses from Figure 8a, the influence of the stack can clearly be observed in Figure 8b. Due to the reverberant incident pulse, the short distance between the microphone and the loudspeaker and the short length of the stack, the different reflections from the stack were hard to separate. Since the first reflections from the loudspeaker arrived at 16.2 ms, the stack reflections are only undisturbed from reflections from the loudspeaker and the open end in the time interval 14.8 ms to 16.2 ms.

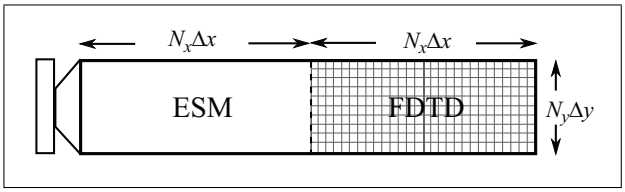

Figure 5. The computational efficiency is investigated by varying the number of grid points N_x and keeping the time and space increment constant.

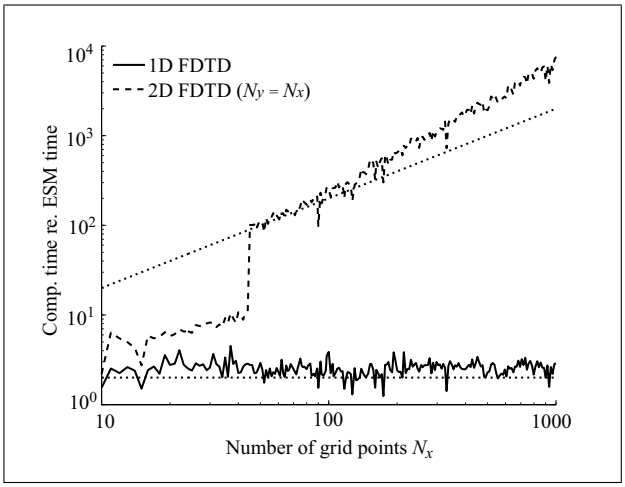

Figure 6. The computational time for 1-D FDTD and 2-D FDTD versus ESM, as function of number of grid points. Quadratic grid, $N_y = N_x$, is assumed for the 2-D FDTD. The dotted diagonal line represents $2N_x$ and the dotted horizontal line represents 2. Damping is excluded in the ESM part.

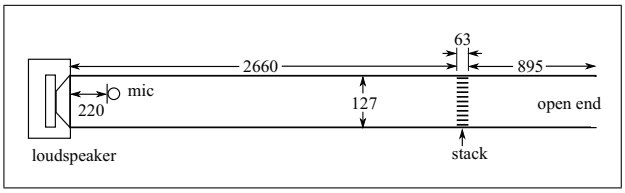

Figure 7. Sketch of the experimental setup. All measurements in millimetres.

5.3. Comparison with analytical expression for area change

Analytical expressions for wave propagation in ducts with area changes, as introduced by the stack, can be found in the literature. For a duct with a cross-section of S_a containing a duct segment with a length L and a different cross-

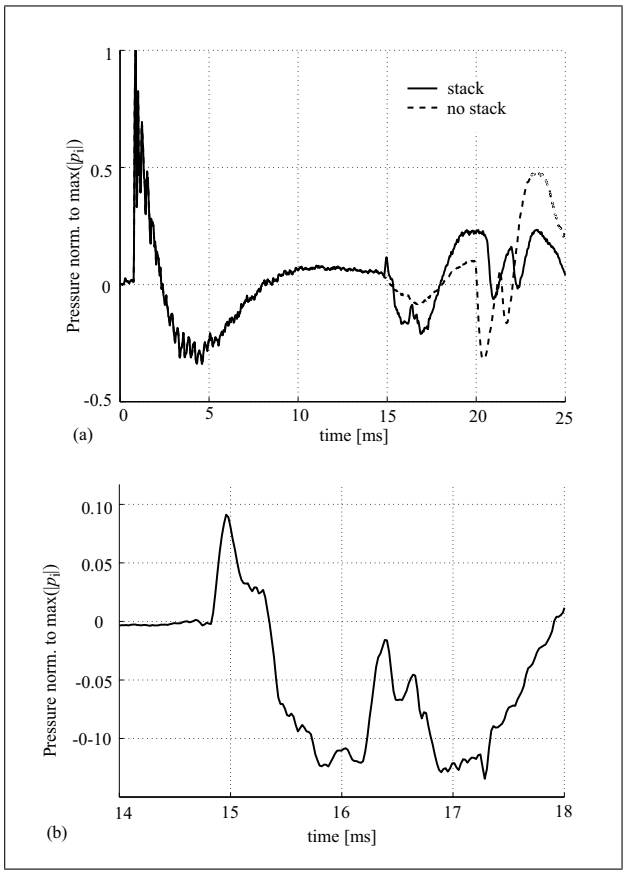

Figure 8. (a) The impulse responses between the microphone signal and the input signal for the two settings, with and without the stack. (b) The subtraction of the impulse responses in (a), zoomed at the reflections from the stack.

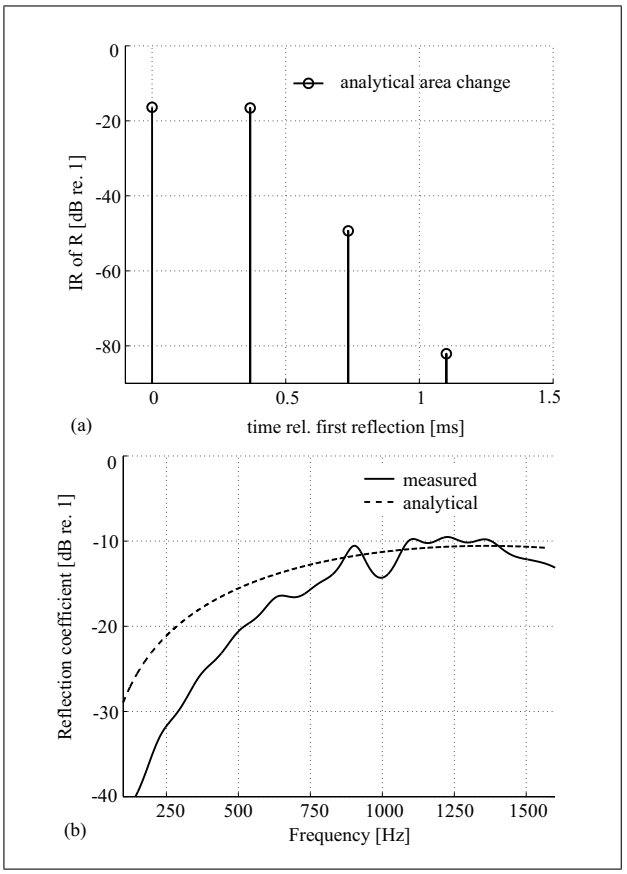

Figure 10. (a) The analytical reflection coefficient for the area changed caused by the stack transformed to the time domain. (b) Comparison between the measured and the analytical reflection coefficients.

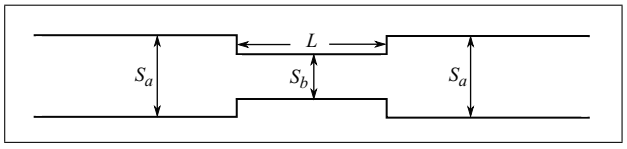

Figure 9. Sketch of two semi-infinite duct segments connected through a finite duct segment with a different cross-section.

section S_b (see Figure 9) the pressure reflection coefficient is described as [19]

$$R = \frac{P_{\text{ref}}}{P_{\text{inc}}} = \frac{\text{j}(S_a/S_b - S_b/S_a)\sin(kL)}{2\cos(kL) + \text{j}(S_a/S_b + S_b/S_a)\sin(kL)}, \quad (26)$$

where P_{ref} is the reflected pressure, P_{inc} the incident pressure and k is the wave number.

The ratio S_b/S_a in equation (26) was replaced by the area change B given in equation (25), so that the analytical reflection coefficient introduced by the stack was calculated. The reflection coefficient was transformed to the time domain, by using the technique described in [20] in order to assure causality and to reduce ripples caused by the Gibbs phenomenon. In addition, the length L was adjusted to fit the time resolution ($\Delta t = 2^{-23}$ s), such that all reflections arrived exactly at a time sample. As seen from the time domain version of the reflection coefficient, Figure 10a, the third reflection is more than 30 dB lower than the second and first reflections. Therefore, the reflection coefficient is mainly determined by the first two reflections.

As a result of the insignificant higher-order reflections, the reflection coefficient was estimated from the first two measured reflections. These two reflections were covered in a time interval of 0.7 ms, from 14.8 ms to 15.5 ms, since the stack had a length of 63 mm. Only reflections from the stack were received in this time interval, since the first reflections from the loudspeaker arrived at 16.2 ms. Thus, the reflected pressure signal was extracted from 14.8 ms to 15.5 ms of the signal in Figure 8b, whereas the incident pressure signal was extracted from 0.7 ms to 7.9 ms of the signal in Figure 8a. These signals were resampled 10 times the original sampling frequency using the Matlab function *resample*. Thereafter, the signals were transformed to the frequency domain using a 2^{19}-point Fast Fourier Transform (*fft* in Matlab) including zero-padding to insure sufficient frequency resolution. The reflection coefficient was calculated by dividing the reflected pressure by the incident pressure in the frequency domain.

Even though the short time interval excluded low frequency content, the resulting reflection coefficient showed good agreement in the higher frequencies with the analyt-

ical expression, as seen in Figure 10b. The reflection coefficient is plotted in the frequency range below the first cross-mode of the duct, which occurs at 1583 Hz.

5.4. Comparison with simulations

The duct containing a stack was modelled using the combination of ESM and 2-D FDTD methods. The loudspeaker and the duct segments at both sides of the stack were modelled by ESM, whereas the stack was modelled by FDTD. In the FDTD part, viscosity caused by the narrow channels was included, as described in the following paragraph.

5.4.1. FDTD discretisation

In addition to the assumptions in sections 2 and 4.2, shear forces in the y-direction were included. Consequently, the acoustic field in the stack was described by the equation of continuity and the momentum equation

$$\frac{\partial p}{\partial t} = -\rho c^2 \frac{\partial u}{\partial x}, \tag{27}$$

$$\frac{\partial u}{\partial t} = -\frac{1}{\rho}\frac{\partial p}{\partial x} + \frac{\mu}{\rho}\frac{\partial^2 u}{\partial y^2}, \tag{28}$$

where μ is the dynamic viscosity and u is the x-component of the velocity. Equations (27) and (28) were discretised with the FDTD method and by introducing sub-volume velocities as described in section 4.2, using a uniform grid with space increment $\delta = \Delta x = \Delta y$. The pressure calculated with central difference of second order at time step n and position (i, j) is

$$p_{i,j}(n+\frac{1}{2}) = p_{i,j}(n-1/2) - \frac{c^2\Delta t}{\delta}\frac{\rho}{\Delta S} \cdot \left[\hat{U}_{i+1/2,j}(n) - \hat{U}_{i-\frac{1}{2},j}(n)\right]. \tag{29}$$

The sub-volume velocity calculated with finite difference at time step $n+\frac{1}{2}$ and position $(i+\frac{1}{2}, j)$ is

$$\begin{aligned}\hat{U}_{i+\frac{1}{2},j}(n+1) &= \hat{U}_{i+\frac{1}{2},j}(n) \\ &- \frac{\Delta t}{\delta\rho/\Delta S}\left[p_{i+1,j}(n+1/2) - p_{i,j}(n+1/2)\right] \\ &+ \frac{\mu\Delta t}{2\delta^2\rho/\Delta S}\left[\hat{U}_{i+\frac{1}{2},j+1}(n+1)\right. \\ &\quad - 2\hat{U}_{i+\frac{1}{2},j}(n+1) + \hat{U}_{i+\frac{1}{2},j-1}(n+1) \\ &\quad \left. + \hat{U}_{i+\frac{1}{2},j+1}(n) - 2\hat{U}_{i+\frac{1}{2},j}(n) + \hat{U}_{i+\frac{1}{2},j-1}(n)\right].\end{aligned} \tag{30}$$

The sub-volume velocities at the transverse ends, $\hat{U}_{i+\frac{1}{2},1}$ and $\hat{U}_{i+\frac{1}{2},N_y}$, are set to zero.

The first derivatives were modelled using a second-order central difference, and the second derivative was modelled using the implicit Crank-Nicholson method and the Thomas algorithm [16]. Since only wave propagation in the x-direction is taken into account, a Courant number equal to one, $S_c = c\Delta t/\delta = 1$, should be applicable. However, simulations with different Courant numbers were tested, in order to study the effects of the numerical reflections, as discussed in section 4.3. The simulations were performed with a grid size of 1677x30 elements, resulting in a time resolution of $1.1 \cdot 10^{-7}$s for $S_c = 1$.

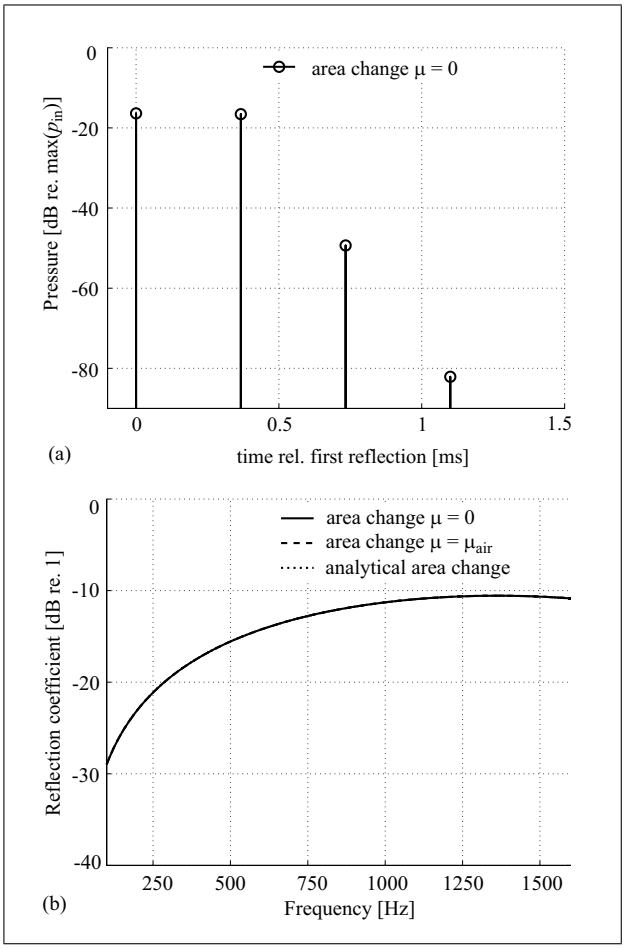

Figure 11. Reflections received Δx away from the stack, using a volume velocity unit pulse and $S_c = 1$. (a) Reflections from the stack, when only area change was included in the simulations. (b) Reflection coefficient R from the stack, plotted as $20\log|R|$. Simulations with and without viscosity and analytical solution for area change are shown. The three lines completely overlap.

5.4.2. Simulation results

In the simulations a volume velocity unit pulse was sent from the ESM part. The pressure reflections from the stack (the FDTD-part) were received at a fixed point Δx away from the stack. The stack reflections are shown in Figure 11a, when only the area change is included. The simulated reflection peaks agree with the analytical reflections in Figure 10a.

The incident and reflected pressure were transformed to the frequency domain by using a 2^{19}-point Fast Fourier Transform, including zero-padding to insure sufficient frequency resolution. The reflection coefficient was calculated by dividing the frequency domain reflected pressure by the incident pressure. As seen in Figure 11b, the analytical and the simulated reflection coefficients for $\mu = 0$ and $\mu = \mu_{air} = 1.837 \cdot 10^{-5}$Pa s in addition to the area change

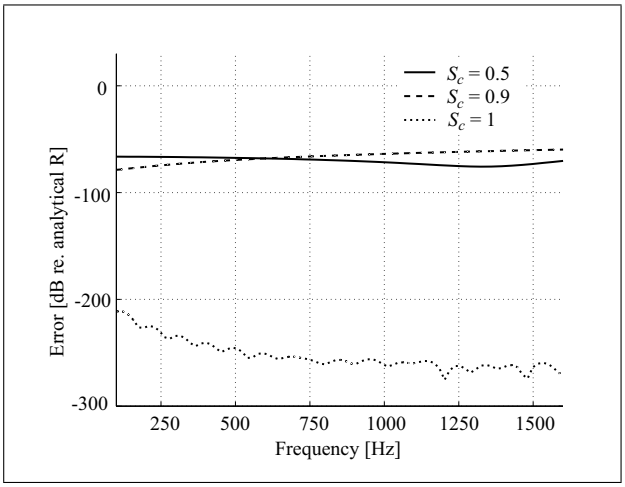

Figure 12. Error relative to analytical reflection coefficient for area change using various Courant numbers.

were practically equal in the valid frequency range. Thus, the coupling between ESM and FDTD seems to work. Furthermore, the viscosity in the channel had an insignificant effect on the reflection coefficient compared to the area change.

In section 4.3, it was shown that simulations with $S_c < 1$ caused numerical reflections. In the simulations of the duct containing a stack, the errors were lower than -60 dB for all tested S_c and -200 dB with $S_c = 1$ in the frequency range of interest, as seen in Figure 12. Thus the numerical errors relative to the analytical reflection coefficient were insignificant in the frequency range of interest.

6. Conclusions

Wave propagation in a duct was modelled using a combination of ESM and FDTD. To our knowledge this was the first time these methods have been combined. The results from simulations agreed well with experimental and analytical results, taking into account the experimental limitations.

Numerical reflections and errors introduced in the coupling between the methods were insignificant in the frequency range of interest, because reflections caused by area change dominated. Thus, the combination of ESM and FDTD is numerically robust and stable, even though no extreme stability test was conducted.

The numerical reflections could be reduced by matching the impedance in the ESM part with the impedance of the FDTD part. However, this impedance matching would be complicated due to the frequency-dependent impedance in the FDTD-part. Moreover, it is not necessary since the numerical errors were insignificant in the frequency range of interest.

The combination of a 1-D with a 2-D formulation reduced the computational cost considerably. Moreover, using the 1-D ESM instead of 1-D FDTD reduced the computational cost by a factor of two. Further improvements in computational efficiency are possible if different time steps in the ESM and the FDTD method can be used. Furthermore, the efficiency in the FDTD part can be improved by exploiting symmetry and non-uniform grids.

The coupling was limited to wave propagation only in the lateral direction; however, expanding to 2-D wave propagation requires a 2-D ESM. Such an expansion would lead to more equivalent sources and complicated Green's functions, resulting in increased complexity of the coupling. The computational cost would only increase proportionally to the lateral resolution.

The current combination of ESM and FDTD is appropriate for modelling the acoustic field in ducts that contain objects of higher complexity. For instance, one application would be thermoacoustic devices, of which the thermoacoustic regenerator or stack could be described by FDTD whereas the simpler parts could be described by ESM.

References

[1] G. W. Swift: Thermoacoustic engines. J. Acoust. Soc. Am. **84** (1988) 1145–1180.

[2] S. L. Garrett: Resource letter: TA-1: Thermoacoustic engines and refrigerators. Am. J. Phys. **72** (2004) 11–17.

[3] W. C. Ward, G. W. Swift: Design environment for low-amplitude thermoacoustic engines. J. Acoust. Soc. Am. **95** (1994) 3671–3672.

[4] D. Botteldooren: Acoustical finite-difference time-domain simulation in a quasi-cartesian grid. J. Acoust. Soc. Am. **95** (1994) 2313–2319.

[5] J. G. Tolan, J. B. Schneider: Locally conformal method for acoustic finite-difference time-domain modeling of rigid surfaces. J. Acoust. Soc. Am. **114** (2003) 2575–2581.

[6] T. Rylander, A. Bondeson: Application of stable FEM–FDTD hybrid to scattering problems. IEEE transactions on antennas and propagation **50** (2002) 141–144.

[7] A. Monorchio, A. R. Bretones, R. Mittra, G. Manara, R. G. Martín: A hybrid time-domain technique that combines the finite element, finite difference and method of moment techniques to solve complex electromagnetic problems. IEEE transactions on antennas and propagation **52** (2004) 2666–2674.

[8] I. Drumm: A hybrid finite element / finite difference time domain technique for modelling the acoustics of surfaces within a medium. Acta Acustica United with Acustica **93** (2007) 804–809.

[9] T. V. Renterghem, E. M. Salomons, D. Botteldooren: Efficient FDTD–PE model for sound propagation in situations with complex abstacles and wind profiles. Acta Acustica United with Acustica **91** (2005) 671–679.

[10] M. Ögren, W. Kropp: Road traffic noise propagation between two dimensional city canyons using an equivalent sources approach. Acta Acustica United With Acustica **90** (2004) 293–300.

[11] M. Hornikx, J. Forssén: The 2.5-dimensional equivalent sources method for directly exposed and shielded urban canyons. J. Acoust. Soc. Am. **122** (2007) 2532–2541.

[12] M. Ochmann: Source simulation technique for acoustic radiation problems. Acustica **81** (1995) 512–527.

[13] W. Kropp, U. P. Svensson: Time domain formulation of the method of equivalent sources. Acta Acustica **3** (1995) 67–73.

[14] W. Kropp, U. P. Svensson: Application of the time domain formulation of the method of equivalent sources to

radiation and scattering problems. Acustica **81** (1995) 528–543.

[15] A. Taflove, S. C. Hagness: Computational electrodynamics: the finite-difference time-domain method. 3 ed. Arctec House Inc., 2005.

[16] J. C. Tannehill, D. A. Anderson, R. H. Pletcher: Computational fluid mechanics and heat transfer. 2 ed. Taylor and Francis, 1997.

[17] K. S. Yee: Numerical solutions of initial boundary value problems involving maxwell's equations in isotropic media. IEEE transactions on antennas and propagation **14** (1966) 302–307.

[18] J. B. Schneider, R. J. Kruhlak: Dispersion of homogeneous and inhomogeneous waves in the Yee finite-difference time-domain grid. IEEE transactions on microwave theory and techniques **49** (2001) 280–287.

[19] L. E. Kinsler, A. R. Frey, A. B. Coppens, J. V. Sanders: Fundamentals of acoustics. 4 ed. John Wiley & Sons, Inc, 2000. Eq. (6.3.7) using $r_1 = r_3 = \rho c/S_a$ and $r_2 = \rho c/S_b$.

[20] P. Andersson: Modelling interfacial details in tyre/road contact - adhesion forces and non-linear contact stiffness. Dissertation. ISBN 91-7291-652-4, Chalmers University of Technology, 2005. Appendix C.